Supporting Information for

Computational and experimental insights into variable temperature propylene (C_3H_6), propane (C_3H_8), and hydrogen sulfide (H_2S) sorption in ultra-high permselectivity CANAL ladder polymers

Brandon C. Tapia[1], Jing Ying Yeo[1], and Zachary P. Smith[*1]

[1]Department of Chemical Engineering, Massachusetts Institute of Technology, Cambridge, Massachusetts 02139, USA

*Corresponding author: Zachary P. Smith (zpsmith@mit.edu)

Contents

S1. Simulation Parameters

S1.1 Polymer Generation

GAFF2 force field parameters were applied to CANAL-Me-Me$_2$F using the Antechamber program within AMBER 14.[1,2] Replacements for missing parameters were automatically chosen using the parmchk2 utility within Antechamber. A skeleton LAMMPS datafile was created for the CANAL-Me-Me$_2$F monomer using the TopoTools plugin within VMD.[3,4]

For polymerization using Polymatic, additional bonding constraints were imposed. Bonds were set to have a maximum length (cutoff radius) of 6 Å with plane constraints less than 40° or greater than 140° and vector constraints greater than 135° as done previously for PIM-1 and explained by Abbott et al.[5]

S1.2 Polymer Relaxation

Table S1. 21-step equilibration procedure where T_{final} is the target temperature of the system (i.e., 308, 328, 398, or 463 K).

Step	Ensemble	Temperature (K)	Pressure (bar)	Duration (fs)
1	NVT	3000	-	50000
2	NVT	T_{final}	-	50000
3	NPT	T_{final}	1000	50000
4	NVT	3000	-	50000
5	NVT	T_{final}	-	100000
6	NPT	T_{final}	30000	50000
7	NVT	3000	-	50000
8	NVT	T_{final}	-	100000
9	NPT	T_{final}	50000	50000
10	NVT	3000	-	50000
11	NVT	T_{final}	-	100000
12	NPT	T_{final}	25000	5000
13	NVT	3000	-	5000
14	NVT	T_{final}	-	10000
15	NPT	T_{final}	5000	5000
16	NVT	3000	-	5000
17	NVT	T_{final}	-	10000
18	NPT	T_{final}	500	5000
19	NVT	3000	-	5000
20	NVT	T_{final}	-	10000
21	NPT	T_{final}	1	800000

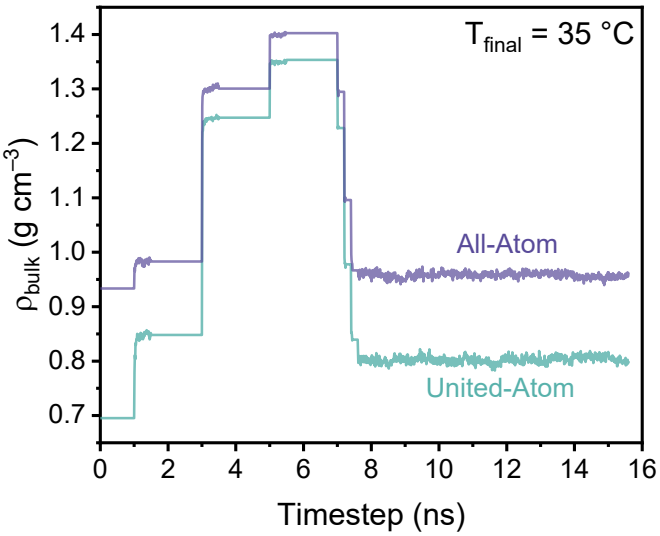

Figure S1. Bulk density versus timestep for the 21-step equilibration procedure of Replicate 1 of CANAL-Me-Me$_2$F for both all-atom (purple) and united-atom (green) systems.

S1.3 H_2S Force Field

As simulated H_2S isotherms exhibited systematic deviation from experimental results, three force field variations for H_2S were trialed to determine whether some showed simulated results that better replicated experimental results. The three force fields variations used are described below.

(1) Modified 4-3 Model from Shah et al.[6]

While the default 4-3 model parameters were used during the GCMC adsorption simulations, gas-phase GCMC simulations utilized a distance between the sulfur and dummy atom (δ_{S-X}) of 0.405 Å compared to the default distance of 0.3 Å. This change was necessary due to errors within the GCMC engine claiming "atom overlap" at smaller distances. The inserted H_2S molecule remained as defined by Shah et al.[6]

(2) 3-3 Model from Shah et al.[6]

(3) 5-1 from Kristóf and Bucsai.[7]

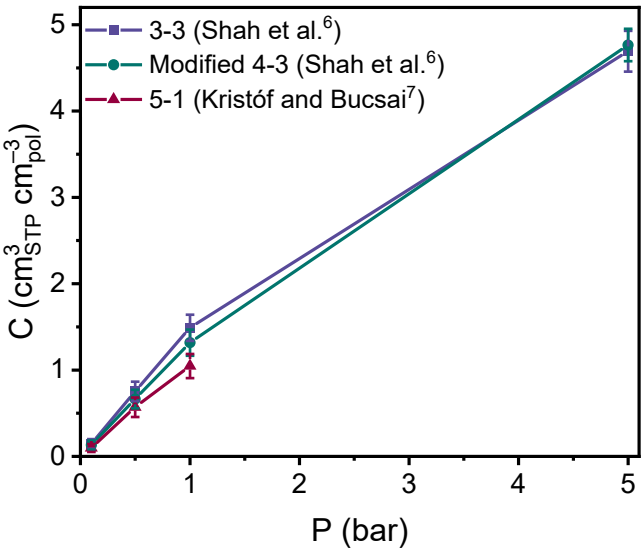

Figure S2. Grand canonical Monte Carlo sorption isotherms of pressure versus concentration for the 3-3 and modified 4-3 H_2S force fields from Shah et al.[6], and the 5-1 H_2S force field from Kristóf and Bucsai.[7] Lines are shown to guide the eye and are not a model fit. The 5-1 force field was not modeled at 5 bar due to no benefit over the less complex force fields at 1 bar.

S1.4 Monte Carlo & Molecular Dynamics Sorption Simulations

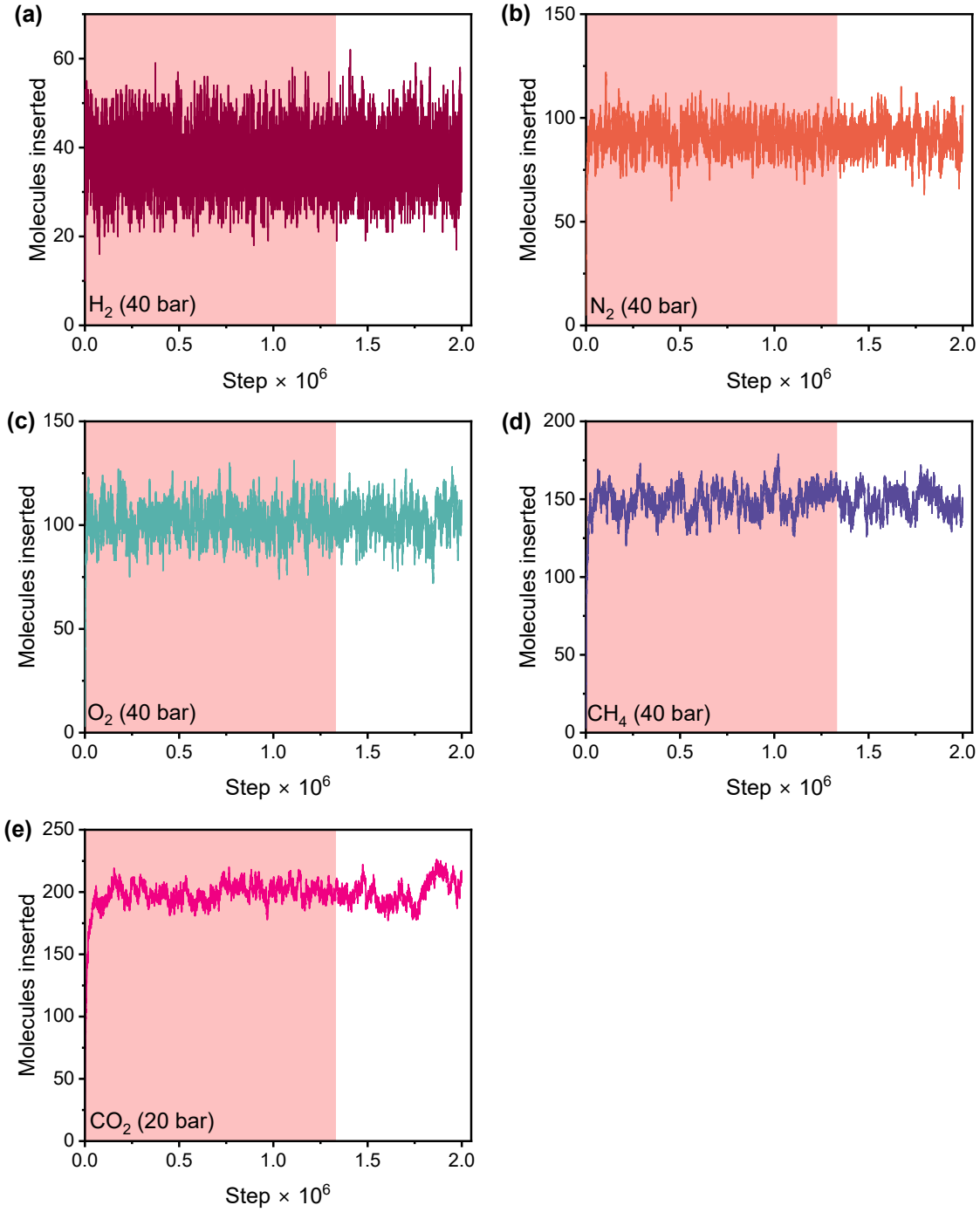

Figure S3. Convergence of molecules inserted in grand canonical Monte Carlo (GCMC) simulations for (a) H_2, (b) N_2, (c) O_2, (d) CH_4, and (e) CO_2 against the number of MC steps. Convergence is shown for the highest pressure datapoint of the respective gas reported in this work, indicated in parentheses within each plot. Data within the shaded red area represents MC steps used to ensure equilibrium and thus was excluded from ensemble averaging. Data is shown for Replicate 1.

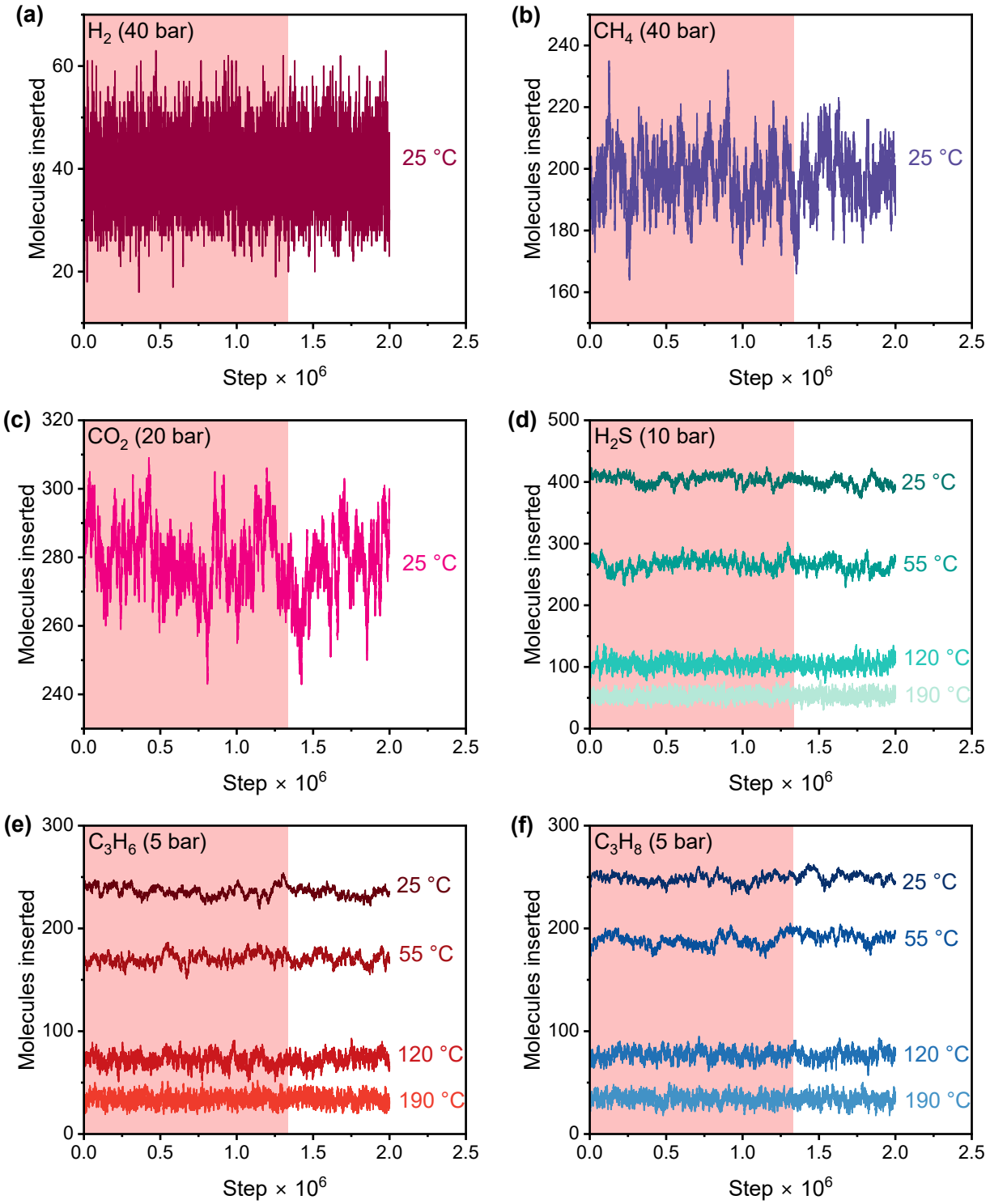

Figure S4. Convergence of molecules inserted in iterated grand canonical Monte Carlo (GCMC) and molecular dynamics (MD) simulations of (a) H_2, (b) CH_4, (c) CO_2, (d) H_2S, (e) C_3H_6, and (f) C_3H_8 against the number of MC steps. Convergence is shown for the highest pressure datapoint, last iteration, and lowest temperature of the respective gas reported in this work. Data within the shaded red area represents MC steps used to ensure equilibrium and thus was excluded from ensemble averaging. Data is shown for Replicate 1.

Table S2. Monte Carlo-molecular dynamics iterations required for convergence between iterations.

Gas	Temperature (K)	Pressure (bar)	Iterations for Convergence
H_2	308	5	10
		10	10
		20	10
		30	10
		40	10
CH_4	308	1	10
		5	10
		10	10
		20	10
		30	10
		40	10
CO_2	308	1	10
		5	10
		10	10
		20	10
C_3H_8	308	0.1	10
		0.5	10
		1	10
		2	10
		3	15
		5	20
	328	0.1	10
		0.5	10
		1	10
		2	10
		3	15
		5	15
	398	0.1	5
		0.5	5
		1	5
		2	5
		3	10
		5	10
	463	0.1	5
		0.5	5
		1	5
		2	5
		3	5
		5	5
C_3H_6	308	0.1	10
		0.5	10
		1	10
		2	10
		3	15
		5	15
	328	0.1	10
		0.5	10
		1	10

Gas	Temperature (K)	Pressure (bar)	Iterations for Convergence
		2	10
		3	15
		5	15
	398	0.1	5
		0.5	5
		1	5
		2	5
		3	10
		5	10
	463	0.1	5
		0.5	5
		1	5
		2	5
		3	5
		5	5
H_2S	308	0.1	5
		0.5	5
		1	5
		2	5
		3	5
		5	5
		10	10
	328	0.1	5
		0.5	5
		1	5
		2	5
		3	5
		5	5
		10	10
	398	0.1	5
		0.5	5
		1	5
		2	5
		3	5
		5	5
		10	5
	463	0.1	5
		0.5	5
		1	5
		2	5
		3	5
		5	5
		10	5

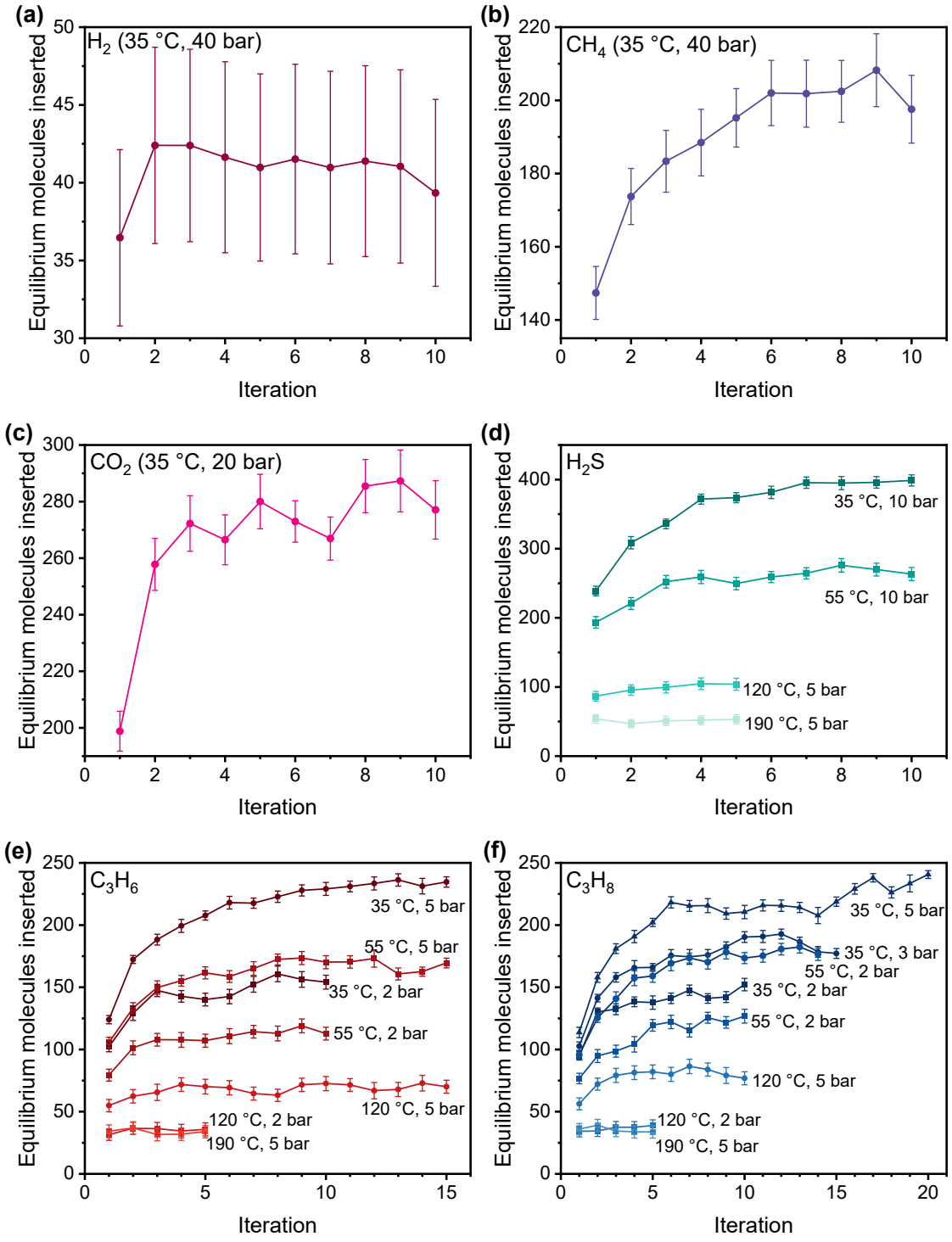

Figure S5. Number of gas molecules inserted at equilibrium versus iteration number at all temperatures reported in this work for (a) H_2, (b) CH_4, (c) CO_2, (d) H_2S, (e) C_3H_6, and (f) C_3H_8. Convergence of iterations is shown for the highest pressure at each number of maximum iterations. For example, for C_3H_8 at 35 °C, 2 bar is shown as the highest pressure that uses 10 iterations, 3 bar is shown as the only pressure that uses 15 iterations, and 5 bar is shown as the only pressure that uses 20 iterations. Other pressures are not shown as it is understood that if higher pressures show convergence at the same number of iterations, lower pressures will as well due to inserting fewer molecules at equilibrium.

S1.5 Modeling CANAL-Me-Me_2F-CN

While not an experimentally synthesized polymer, a CANAL-Me-Me_2F-like polymer containing nitrile groups was simulated to better understand the energetics of how CANAL-Me-Me_2F compared to PIM-1. All polymer system generation, gas models, and MC and MD simulations were performed as described previously, except for the changes noted below:

(1) New versions of LAMMPS (29 August 2024) and Cassandra (version 1.3.0) were used due to updates in the computing environments.

(2) During MCMD simulations, the number of Monte Carlo trials per iteration was reduced from 2,000,000 steps to 1,000,000 steps for pressures of 0.5–5 bar at 338 K and all pressures at 398 K and 463 K. This change was implemented due to the extensive resource usage of these simulations. This change is not expected to cause any changes as these MCMD simulations are run well past their equilibrium point. All MD iterations kept the same setting as done previously (2,000,000 steps with a 0.5-fs timestep).

(3) The number of iterations for convergence for C_3H_8 and C_3H_6 at 328 K and 0.1 bar and 0.5 bar was reduced from 10 to 5 iterations.

S1.6 Calibration Mapping of Chemical Potential to Pressure

To map chemical potential to pressure, bulk gas phase GCMC simulations were performed at multiple pressures for each temperature pair as employed in previous studies.[8–10] These chemical potential-pressure calibration curves were then fit to the functional form

$$\mu(p_i) = \alpha \ln\left(\frac{p_i}{p_0}\right) - \beta \tag{S1}$$

where μ is the chemical potential of the gas, p_i is the partial pressure of the gas, p_0 is the reference pressure of 1 bar, and α and β are fitted parameters. Results were validated against previously published chemical potentials to pressure fits by Morgan et al.[11]

Table S3. Pressure mapped to chemical potential for all gas–temperature conditions studied.

Gas	Temperature (K)	α (kJ mol^{-1})	β (kJ mol^{-1})
H_2	308	2.6085	30.1231
N_2	308	2.5993	40.2362
O_2	308	2.6002	40.7719
CH_4	308	2.5723	38.1195
CO_2	308	2.5321	42.0002
H_2S	308	2.7575	41.3794
	328	2.6898	44.1314
	398	3.6257	55.5555
	463	4.3729	66.1624
C_3H_8	308	2.4698	42.1687
	328	2.6674	45.3100
	398	3.5215	56.8178
	463	4.2036	67.6328
C_3H_6	308	2.4997	41.9215
	328	2.6831	45.0837
	398	3.5471	56.5990
	463	4.2324	67.3651

S2. Polymer Morphology

S2.1 Volumetric Thermal Expansion Coefficient

Equation 13 is derived as:

$$\alpha_V = \frac{1}{V}\left(\frac{\partial V}{\partial T}\right)_P = \frac{\rho}{m}\left(\frac{\partial \frac{m}{\rho}}{\partial T}\right)_P = \rho\left(\frac{\partial \rho^{-1}}{\partial T}\right)_P = -\frac{\rho}{\rho^2}\left(\frac{\partial \rho}{\partial T}\right)_P = -\frac{1}{\rho}\left(\frac{\partial \rho}{\partial T}\right)_P \tag{S2}$$

The approximation utilized is derived as

$$\alpha_V \int_{T_o}^{T} dt = \int_{V_o}^{V_0+\Delta V} \frac{1}{V} dV \Rightarrow \alpha_V \Delta T = \ln\left(1 + \frac{\Delta V}{V_0}\right) \tag{S3}$$

where for $\frac{\Delta V}{V_0} \ll 1$, a Taylor expansion yields

$$\ln\left(1 + \frac{\Delta V}{V_0}\right) \approx \frac{\Delta V}{V_0} \tag{S4}$$

and thus,

$$\alpha_V = \frac{1}{V_0}\frac{\Delta V}{\Delta T} \tag{S5}$$

Due to the non-linearity within the experimental data, it was fit to a third-order polynomial, shown in **Figure S6** to extract the expansion coefficient without relying on the linear approximation.

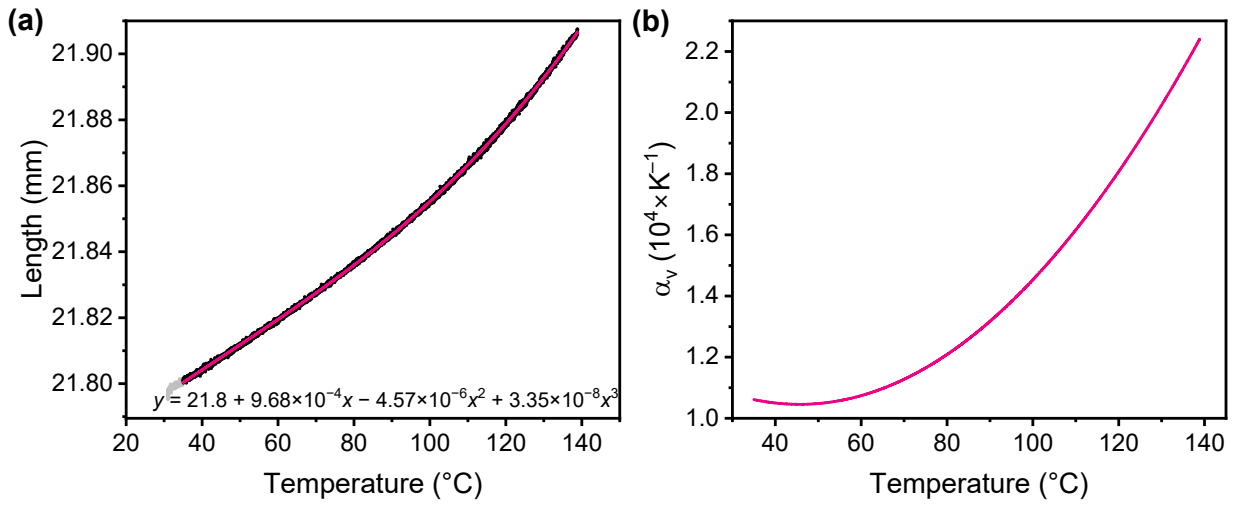

Figure S6. (a) Length of CANAL-Me-Me_2F versus temperature from dynamic mechanical analysis (DMA) experiments. The black data represents data used to determine the expansion coefficient, the gray data represents data excluded from the fitting, and the pink line represents the fit to the data with the third-order polynomial shown in (a). (b) The thermal volumetric expansion coefficient calculated from the length versus temperature data, assuming isotropic expansion.

S2.2 PoreBlazer Settings

The `defaults.dat` file provided with PoreBlazer was used with minor modifications, highlighted in red, shown below:

```
ff.atoms
2.58, 10.22, 298, 12.8
probe_diameter
500
0.2
15, bin_size
21908391
0
```

Rather than use the default Universal force field (UFF)[12] provided with PoreBlazer in `uff.atoms`, intramolecular parameters were taken from either the TraPPE-UA or GAFF2 force fields for UA and AA systems, respectively, to maintain consistency with the MD and MC simulations described in the main text. The probe diameter was varied to measure volume accessible to different gases. Probes with the kinetic diameters of He (d=2.60 Å), CO_2 (d=3.30 Å), O_2 (d=3.46 Å), N_2 (d=3.64 Å), and CH_4 (d=3.80 Å) were used.[13] An additional probe (d=0.10 Å) was used to analyze smaller FVEs. The bin size was kept at the default value of 0.25 Å for visualizing FVDs as smaller bin sizes introduced additional noise, however, was

set at 0.01 Å when computing properties reliant on the cumulative FVD (e.g., minimum and maximum FVE sizes) to increase precision.

S2.3 Free Volume Distribution (FVD)

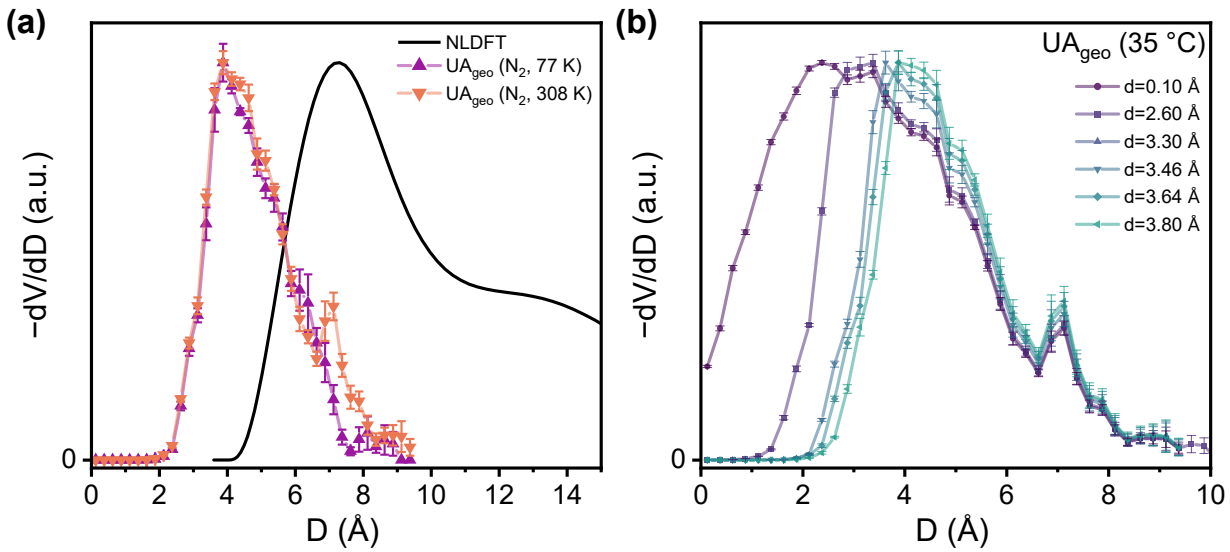

Figure S7. (a) Free volume distribution (FVD) of CANAL-Me-Me$_2$F from non-local density functional theory (NLDFT) via experimental N_2 sorption measurements at 77 K as well as simulated geometric determination from united-atom (UA) simulations at 35 °C and 77 K using an N_2 probe. (b) FVD of CANAL-Me-Me$_2$F from UA simulations at 35 °C using probes of different diameters. Solid lines are meant to guide the eyes.

S2.4 Fractional Free Volume (FFV)

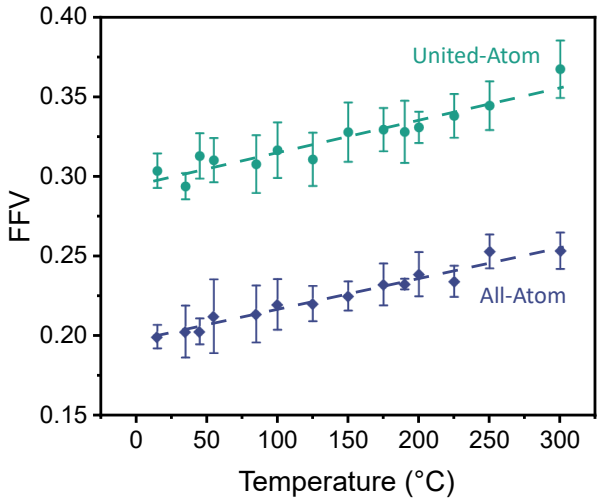

Figure S8. Simulated fractional free volume (FFV) using a helium probe versus temperature for the united-atom and all-atom CANAL-Me-Me$_2$F systems, computed with PoreBlazer.

S2.5 Static Structure Factor (S(q))

The static structure factor ($S(q)$) is defined through the Fourier transform of the radial distribution function (RDF) as

$$S(q) = 1 + 4\pi\rho \int_0^\infty \frac{\sin(qr)}{qr} (g(r) - 1)\, r^2\, dr \quad \text{(S6)}$$

where $q = 2\pi/d$ (where d is distance), ρ is bulk density, and $g(r)$ is the RDF which represents the probability of finding another atom in a shell dr at distance r from a reference atom. Further details are available in the paper introducing the ISAACS program by Le Roux and Petkov.[14]

S2.6 Density

All experimental and simulated sorption isotherms for CANAL-Me-Me_2F are calculated using a density of 0.96 ± 0.02 g cm^{-3} that was determined in this study. This is within uncertainty of a previously determined density of CANAL-Me-Me_2F of 1.01 ± 0.06 g cm^{-3} that has been used previously.[15]

S3. Gas Sorption

S3.1 All-Atom Sorption Isotherms

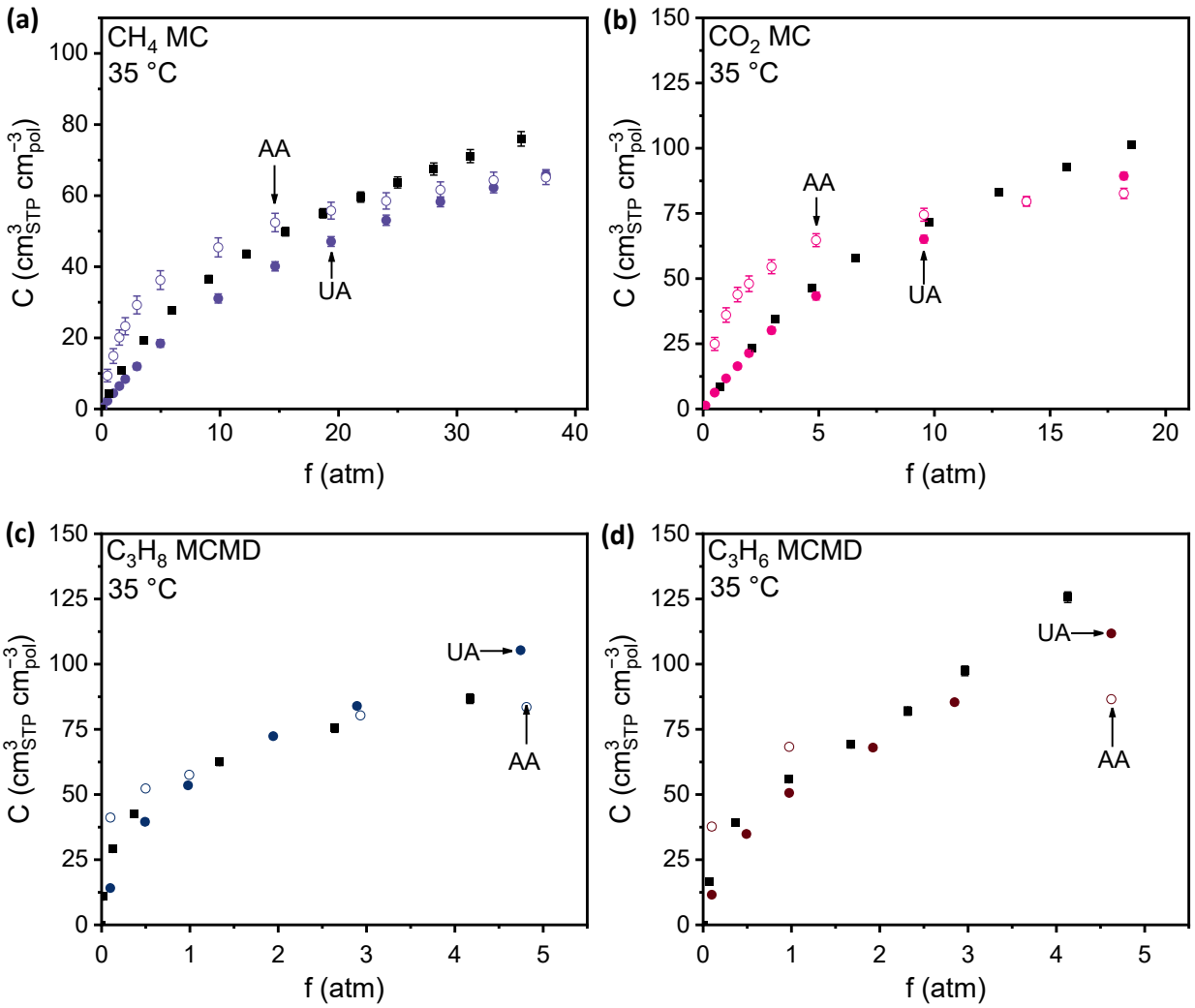

Figure S9. Experimental (squares), all-atom (AA) (unfilled circles) and united-atom (UA) (filled circles) sorption isotherms of (a) CH_4, (b) CO_2 at 35 °C, (c) C_3H_8, and (d) C_3H_6. AA results were not seen to outperform UA data and due to their increased computational resources, were not pursued further. As only one replicate was performed, uncertainty is reported as the standard deviation of the equilibrium fluctuations.

S3.2 Linear Free Energy Relationship (LFER) Constrained Dual-Mode Sorption (DMS) Model

The dual-mode sorption (DMS) model was fit using a linear free energy constrained model, developed by Wu et al.[16] The fitting was performed using a Python program, pyDMS, currently being developed in the Smith Lab at the Massachusetts Institute of Technology. While public release is anticipated shortly, the pre-release version is available by contacting the corresponding author.

The constraints within the model fix the enthalpies of Henry sorption (ΔH_D) and Langmuir sorption (ΔH_b) to linear free energy relationships (LFERs) as

$$\Delta H_\mathrm{D} = \alpha_\mathrm{D} \ln\left(k_{\mathrm{D},0}\right) + \beta_\mathrm{D} \tag{S7}$$

and

$$\Delta H_\mathrm{b} = \alpha_\mathrm{b} \ln(k_{\mathrm{b},0}) + \beta_\mathrm{b} \tag{S8}$$

respectively, where α_D, β_D, α_b, and β_b are fitted parameters. **Table S4** and **Table S5** show the bounds on the constraints and the initial guesses for CANAL-Me-Me$_2$F, PIM-1, and CANAL-Me-Me$_2$F-CN.

Table S4. Upper and lower bound range for initial guesses and optimization constraints for $k_{\mathrm{D},0}$, ΔH_D, b_0, and ΔH_b.

Parameter	Constraint Range [lower bound, upper bound]	Initial Guess Range [lower guess, upper guess]
$k_{\mathrm{D},0}$ (kJ mol^{-1})	[0, ∞]	[0.001, 0.01]
ΔH_D (kJ mol^{-1})	[−50, 0]	[−1, −30]
b_0 (kJ mol^{-1})	[0, ∞]	[0.0001, 0.005]
ΔH_b (kJ mol^{-1})	[−50, 0]	[−1, −30]

Table S5. Upper and lower bound range for initial guesses and optimization constraints for C'_H at each temperature studied.

Polymer	Temperature (°C)	C'_H (cm^3_{STP} cm^{-3}_{pol}) [lower bound, upper bound]	C'_H (cm^3_{STP} cm^{-3}_{pol}) [lower guess, upper guess]
CANAL-Me-Me_2F	35	[0, 100]	[0, 70]
	55	[0, 90]	[0, 70]
	125	[0, 40]	[0, 30]
	190	[0, 0.0001]	[0, 0.00001]
CANAL-Me-Me_2F-CN	35	[0, 100]	[0, 70]
	55	[0, 90]	[0, 70]
	125	[0, 40]	[0, 30]
	190	[0, 0.0001]	[0, 0.00001]
PIM-1	25	[0, 150]	[0, 100]
	35	[0, 150]	[0, 100]
	45	[0, 150]	[0, 100]
	55	[0, 150]	[0, 100]
	65	[0, 150]	[0, 100]

Justification for these constraints largely follows that of Wu et al.[16] and Dean et al.[17] As there have been conflicting reports on the temperature dependence of C'_H (e.g., linear[18] or van't Hoff[19]), the only constraint applied to C'_H was that it must decrease with increasing temperature. Past a certain temperature, Langmuir sorption is no longer visible, and isotherms appear linear. The model, however, does not have a built-in mechanism to recognize this feature, thus it is possible for the model to assign values to C'_H even where sorption is linear, representing a pseudo-Henry's constant of[18]

$$k_D^* = k_D + C'_H b \tag{S9}$$

For linear sorption isotherms, C'_H was constrained such that it was negligible (<0.0001) and $C'_H b$ was thus negligible as well. Note that the same results can be determined whether C'_H is constrained to be negligible or not. This constraint simply aids in data analysis as

$$k_D^* = k_D \tag{S10}$$

S3.3 Dual-Mode Sorption (DMS) Parameters and Analysis

Table S6. Contribution of infinite sorption decoupled into the Langmuir and Henry modes

	Gas	Temperature (°C)	S_∞ ($cm^3_{STP}\ cm^{-3}_{pol}\ atm^{-1}$)	$\frac{S_{\infty,Langmuir}}{S_\infty}$
CANAL-Me-Me$_2$F	H_2S	35	33 ± 1	0.59 ± 0.02
		55	21 ± 1	0.53 ± 0.04
		125	6 ± 1	0.3 ± 0.1
		190	2.3 ± 0.4	0.00 ± 0.03
	C_3H_8	35	172 ± 2	0.94 ± 0.03
		55	90 ± 1	0.91 ± 0.01
		125	13 ± 1	0.6 ± 0.1
		190	4 ± 1	0.0 ± 0.1
	C_3H_6	35	141 ± 2	0.90 ± 0.03
		55	75 ± 1	0.86 ± 0.01
		125	11 ± 1	0.5 ± 0.1
		190	3 ± 1	0.0 ± 0.1
PIM-1	H_2S	35	158 ± 1	0.92 ± 0.01
		45	114 ± 1	0.91 ± 0.01
		55	82 ± 1	0.90 ± 0.01
		65	62 ± 1	0.89 ± 0.02
	C_3H_8	25	361 ± 2	0.97 ± 0.02
		35	286 ± 1	0.97 ± 0.01
		45	235 ± 1	0.97 ± 0.01
		55	184 ± 1	0.97 ± 0.01
	C_3H_6	25	486 ± 2	0.97 ± 0.01
		35	289 ± 1	0.97 ± 0.01
		45	181 ± 1	0.96 ± 0.01
		55	120 ± 1	0.95 ± 0.02

Table S7. Dual-mode sorption parameters for PIM-1 recomputed using the LFER-constrained DMS model along with the original DMS parameters from Li et al.[20]

	Gas	Temperature (°C)	k_D ($cm^3_{STP}\ cm^{-3}_{pol}\ atm^{-1}$)	C'_H ($cm^3_{STP}\ cm^{-3}_{pol}$)	b (atm^{-1})
LFER-Constrained	C_3H_8	25	11.9 ± 0.3	72 ±1	4.9 ±0.2
		35	8.9 ± 0.1	67 ±1	4.1 ±0.1
		45	6.8 ± 0.1	64 ±1	3.57±0.01
		55	5.3 ± 0.1	58 ±1	3.1 ±0.1
	C_3H_6	25	12.8 ± 0.2	74.6±0.2	6.34±0.05
		35	9.6 ± 0.1	68.4±0.3	4.08±0.03
		45	7.3 ± 0.1	64.1±0.3	2.71±0.02
		55	5.7 ± 0.1	62.3±0.4	1.84±0.02
Original	C_3H_8	25	10.5	78.1	3.43
		35	7.82	70.4	4.04
		45	6.4	65.5	3.52
		55	4.89	59.3	3.05
	C_3H_6	25	10.1	88.8	2.57
		35	7.26	81.1	2.36
		45	5.16	78.0	1.64
		55	5.09	63.2	2.09

Table S8. Dual-mode sorption parameters for CANAL-Me-Me$_2$F-CN computed using the LFER-constrained DMS model.

	Gas	Temperature (°C)	k_D ($cm^3_{STP}\ cm^{-3}_{pol}\ atm^{-1}$)	C'_H ($cm^3_{STP}\ cm^{-3}_{pol}$)	b (atm^{-1})
CANAL-Me-Me$_2$F-CN	C_3H_8	35	13.3 ± 0.1	90 ± 1	0.534 ± 0.004
		55	9.9 ± 0.1	61 ± 1	0.400 ± 0.003
		125	4.48 ± 0.02	18 ± 2	0.18 ± 0.01
		190	2.65 ± 0.01	0 ± 1	0.11 ± 0.01
	C_3H_6	35	10.7 ± 0.2	44 ± 1	3.5 ± 0.1
		55	8.4 ± 0.1	38 ± 1	1.63 ± 0.03
		125	4.3 ± 0.1	23 ± 2	0.20 ± 0.01
		190	2.8 ± 0.1	0 ± 3	0.051 ± 0.003
	C_3H_8	35	7.9 ± 0.1	50 ± 1	3.8 ± 0.1
		55	6.6 ± 0.1	42.9 ± 0.4	1.91 ± 0.02
		125	4.11 ± 0.01	22 ± 1	0.30 ± 0.01
		190	3.01 ± 0.04	0 ± 1	0.09 ± 0.01

Table S9. Heats of overall ($\Delta H_{S,\infty}$), Henry (ΔH_D), and Langmuir sorption (ΔH_b) for C_3H_8 and C_3H_6 in PIM-1 using the original DMS parameters by Li et al.[20] Data in parenthesis indicates the percent difference from the LFER-constrained model values.

Gas	$\Delta H_{S,\infty}$ (kJ mol^{-1})	ΔH_D (kJ mol^{-1})	ΔH_b (kJ mol^{-1})
C_3H_8	−11 ± 4 (45%)	−20 ± 1 (8%)	−4 ± 4 (105%)
C_3H_6	−17 ± 4 (77%)	−20 ± 4 (12%)	−8 ± 7 (122%)

Table S10. Heats of overall ($\Delta H_{S,\infty}$), Henry (ΔH_D), and Langmuir sorption (ΔH_b) for H_2S, C_3H_8, and C_3H_6 in CANAL-Me-Me$_2$F-CN.

Gas	$\Delta H_{S,\infty}$ (kJ mol^{-1})	ΔH_D (kJ mol^{-1})	ΔH_b (kJ mol^{-1})
H_2S	−23.9 ± 0.4	−12.4 ± 0.1	−12 ± 1
C_3H_8	−32.0 ± 0.4	−7.3 ± 0.2	−29 ± 1
C_3H_6	−31 ± 1	−10 ± 1	−32 ± 1

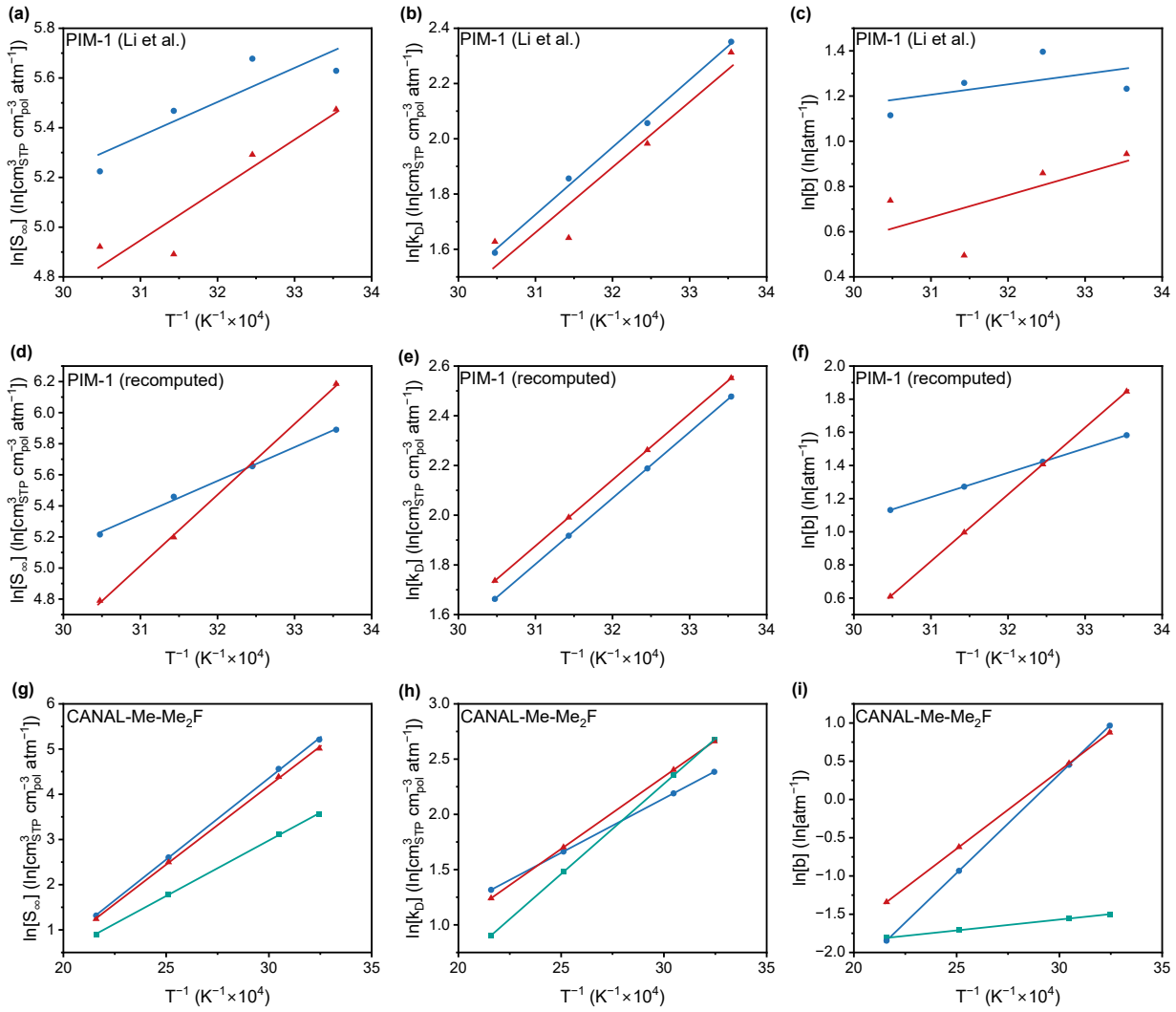

Figure S10. Linearized regressions of $S_{\infty,0}$, k_D and b versus inverse thermal energy for C_3H_8 (blue circles) and C_3H_6 (red triangles) in (a–c) PIM-1 from Li et al.[20], (d–e) the same PIM-1 data reanalyzed with the LFER-constrained DMS model, and (g–i) for H_2S (green squares), C_3H_8 (blue circles), and C_3H_6 (red triangles) in CANAL-Me-Me$_2$F.

S4. Literature Data Extraction

WAXS data from Lai et al.[21] and sorption isotherms from Li et al.[20] utilized in this paper were only available in graphical form. To extract these data, the free online PlotDigitizer software[22] was used, which has been previously validated.[23]

References

(1) Case, D. A.; Aktulga, H. M.; Belfon, K.; Cerutti, D. S.; Cisneros, G. A.; Cruzeiro, V. W. D.; Forouzesh, N.; Giese, T. J.; Götz, A. W.; Gohlke, H.; Izadi, S.; Kasavajhala, K.; Kaymak, M. C.; King, E.; Kurtzman, T.; Lee, T.-S.; Li, P.; Liu, J.; Luchko, T.; Luo, R.; Manathunga, M.; Machado, M. R.; Nguyen, H. M.; O'Hearn, K. A.; Onufriev, A. V.; Pan, F.; Pantano, S.; Qi, R.; Rahnamoun, A.; Risheh, A.; Schott-Verdugo, S.; Shajan, A.; Swails, J.; Wang, J.; Wei, H.; Wu, X.; Wu, Y.; Zhang, S.; Zhao, S.; Zhu, Q.; Cheatham, T. E. I.; Roe, D. R.; Roitberg, A.; Simmerling, C.; York, D. M.; Nagan, M. C.; Merz, K. M. Jr. AmberTools. *J. Chem. Inf. Model.* **2023**, *63* (20), 6183–6191. https://doi.org/10.1021/acs.jcim.3c01153.

(2) D.A. Case; H.M. Aktulga; K. Belfon; I.Y. Ben-Shalom; J.T. Berryman; S.R. Brozell; D.S. Cerutti; T.E. Cheatham; III; G.A. Cisneros; V.W.D. Cruzeiro; T.A. Darden; N. Forouzesh; M. Ghazimirsaeed; G. Giambaşu; T. Giese; M.K. Gilson; H. Gohlke; A.W. Goetz; J. Harris; Z. Huang; S. Izadi; S.A. Izmailov; K. Kasavajhala; M.C. Kaymak; A. Kovalenko; T. Kurtzman; T.S. Lee; P. Li; Z. Li; C. Lin; J. Liu; T. Luchko; R. Luo; M. Machado; M. Manathunga; K.M. Merz; Y. Miao; O. Mikhailovskii; G. Monard; H. Nguyen; K.A. O'Hearn; A. Onufriev; F. Pan; S. Pantano; A. Rahnamoun; D.R. Roe; A. Roitberg; C. Sagui; S. Schott-Verdugo; A. Shajan; J. Shen; C.L. Simmerling; N.R. Skrynnikov; J. Smith; J. Swails; R.C. Walker; J. Wang; J. Wang; X. Wu; Y. Wu; Y. Xiong; Y. Xue; D.M. York; C. Zhao; Q. Zhu; and P.A. Kollman. AMBER 14, 2014.

(3) Alex Kohlmeyer; Josh Vermaas. TopoTools, 2021.

(4) Humphrey, W.; Dalke, A.; Schulten, K. VMD: Visual molecular dynamics. *J. Mol. Graph.* **1996**, *14* (1), 33–38. https://doi.org/10.1016/0263-7855(96)00018-5.

(5) Abbott, L. J.; Hart, K. E.; Colina, C. M. Polymatic: a generalized simulated polymerization algorithm for amorphous polymers. *Theor. Chem. Acc.* **2013**, *132* (3), 1334. https://doi.org/10.1007/s00214-013-1334-z.

(6) Shah, M. S.; Tsapatsis, M.; Siepmann, J. I. Development of the transferable potentials for phase equilibria model for hydrogen sulfide. *J. Phys. Chem. B* **2015**, *119* (23), 7041–7052. https://doi.org/10.1021/acs.jpcb.5b02536.

(7) Kristóf, T.; Bucsai, D. Atomistic simulation study of the adsorptive separation of hydrogen sulphide/alkane mixtures on all-silica zeolites. *Mol. Sim.* **2022**, *48* (1), 31–42. https://doi.org/10.1080/08927022.2021.1914336.

(8) Kupgan, G.; Demidov, A. G.; Colina, C. M. Plasticization behavior in polymers of intrinsic microporosity (PIM-1): A simulation study from combined Monte Carlo and molecular dynamics. *J. Membr. Sci.* **2018**, *565*, 95–103. https://doi.org/10.1016/j.memsci.2018.08.004.

(9) Anstine, D. M.; Demidov, A. G.; Mendez, N. F.; Morgan, W. J.; Colina, C. M. Screening PIM-1 performance as a membrane for binary mixture separation of gaseous organic compounds. *J. Membr. Sci.* **2020**, *599*, 117798. https://doi.org/10.1016/j.memsci.2019.117798.

(10) *Cassandra*. https://sites.nd.edu/maginn-group/cassandra/ (accessed 2024-11-21).

(11) Morgan, W. J.; Anstine, D. M.; Colina, C. M. Temperature effects in flexible adsorption processes for amorphous microporous polymers. *J. Phys. Chem. B* **2022**, *126* (33), 6354–6365. https://doi.org/10.1021/acs.jpcb.2c04543.

(12) Rappe, A. K.; Casewit, C. J.; Colwell, K. S.; Goddard III, W. A.; Skiff, W. M. UFF, a full periodic table force field for molecular mechanics and molecular dynamics simulations. *J. Am. Chem. Soc.* **1992**, *114* (25), 10024–10035. https://doi.org/10.1021/ja00051a040.

(13) Shieh, J.-J.; Chung, T. S. Gas permeability, diffusivity, and solubility of poly(4-vinylpyridine) film. *J. Polym. Sci., Part B: Polym. Phys.* **1999**, *37* (20), 2851–2861. https://doi.org/10.1002/(SICI)1099-0488(19991015)37:20%253C2851::AID-POLB5%253E3.0.CO;2-U.

(14) Le Roux, S.; Petkov, V. ISAACS – interactive structure analysis of amorphous and crystalline systems. *J. Appl. Crystallogr.* **2010**, *43* (1), 181–185. https://doi.org/10.1107/s0021889809051929.

(15) Yeo, J. Y.; Benedetti, F. M.; Pedretti, B.; Robinson, A. M.; Yin, R.; Lai, H. W. H.; Lee, T. H.; Xia, Y.; Smith, Z. P. Investigation of competitive sorption and plasticization of hyperaged CANAL ladder polymers for acid gas purification. *J. Membr. Sci.* **2025**, 123973. https://doi.org/10.1016/j.memsci.2025.123973.

(16) Wu, A. X.; Drayton, J. A.; Mizrahi Rodriguez, K.; Benedetti, F. M.; Qian, Q.; Lin, S.; Smith, Z. P. Elucidating the role of fluorine content on gas sorption properties of fluorinated polyimides. *Macromolecules* **2021**, *54* (1), 22–34. https://doi.org/10.1021/acs.macromol.0c01746.

(17) Dean, P. A.; Mizrahi Rodriguez, K.; Guo, S.; Roy, N.; Swager, T. M.; Smith, Z. P. Elucidating the role of micropore-generating backbone motifs and amine functionality on H_2S, CO_2, CH_4 and N_2 sorption. *J. Membr. Sci.* **2024**, *696*, 122465. https://doi.org/10.1016/j.memsci.2024.122465.

(18) Koros, W. J.; Paul, D. R. CO_2 sorption in poly(ethylene terephthalate) above and below the glass transition. *J. Polym. Sci.: Polym. Phy. Ed.* **1978**, *16* (11), 1947–1963. https://doi.org/10.1002/pol.1978.180161105.

(19) Koros, W. J.; Paul, D. R.; Huvard, G. S. Energetics of gas sorption in glassy polymers. *Polymer* **1979**, *20* (8), 956–960. https://doi.org/10.1016/0032-3861(79)90192-7.

(20) Li, P.; Chung, T. S.; Paul, D. R. Temperature dependence of gas sorption and permeation in PIM-1. *J. Membr. Sci.* **2014**, *450*, 380–388. https://doi.org/10.1016/j.memsci.2013.09.030.

(21) Lai, H. W. H.; Benedetti, F. M.; Ahn, J. M.; Robinson, A. M.; Wang, Y.; Pinnau, I.; Smith, Z. P.; Xia, Y. Hydrocarbon ladder polymers with ultrahigh permselectivity for membrane gas separations. *Science* **2022**, *375* (6587), 1390–1392. https://doi.org/10.1126/science.abl7163.

(22) *PlotDigitizer*. https://plotdigitizer.com/app (accessed 2025-05-30).

(23) Aydin, O.; Yassikaya, M. Y. Validity and reliability analysis of the PlotDigitizer software program for data extraction from single-case graphs. *Perspect. Behav. Sci.* **2022**, *45* (1), 239–257. https://doi.org/10.1007/s40614-021-00284-0.